JOURNAL OF SOLID STATE CHEMISTRY 92, 460–472 (1991)

An Electron and X-Ray Diffraction Study of L-Ta_2O_5-Type Phases in L-Ta_2O_5 and Some L-Ta_2O_5–M_aO_b Systems: (M = Al, Ti, Zr, Hf, W)

J. M. WILLIAMS, R. J. D. TILLEY*, G. HARBURN, AND R. P. WILLIAMS

*Department of Physics and *Division of Materials, School of Engineering, University of Wales College of Cardiff, P.O. Box 917, Cardiff CF2 1XH, United Kingdom*

Received October 24, 1990

An electron and X-ray diffraction study of L-Ta_2O_5-type phases in L-Ta_2O_5 and the L-Ta_2O_5-WO_3, L-Ta_2O_5-ZrO_2, L-Ta_2O_5-HfO_2, L-Ta_2O_5-Al_2O_3, and L-Ta_2O_5-TiO_2 systems is reported. A continuum of structures which evolve with oxygen content has been found, most of which display incommensurability along b^*. These incommensurate diffraction patterns, simulated by an intergrowth model using structural units of 13, 16, 19, . . . 31, 34, are found to be the norm and no special significance is attached to L-Ta_2O_5 as such. The compounds conform to the description "infinitely adaptive" phases.

Introduction

The low-temperature polymorph of tantalum pentoxide, L-Ta_2O_5, has proved extremely difficult to characterize structurally, despite its simple stoichiometric formula. The unit cell of L-Ta_2O_5 has been found to be very large in the b direction and this parameter appears to vary both with temperature and sample preparation and with impurity content. Similar complexity exists in ternary L-Ta_2O_5-related phases found in the L-Ta_2O_5–Al_2O_3, L-Ta_2O_5–TiO_2, L-Ta_2O_5–ZrO_2, and L-Ta_2O_5–WO_3 systems (1). It is therefore more satisfactory to consider the L-Ta_2O_5 related structures as a set of infinitely adaptive phases (2).

The compounds possess an orthorhombic subcell with $a' \approx 0.62$ nm, $b' \approx 0.366$ nm, $c' \approx 0.389$ nm (*3*), but X-ray powder patterns also contain numerous weak superstructure lines, one of which, the "c-line" was used by Moser (*4*) to characterize individual samples. The situation was greatly clarified by Stephenson and Roth (*5–8*) who determined the structures of several phases in the L-Ta_2O_5–WO_3 system using single crystal X-ray diffraction techniques. These phases had orthorhombic unit cells with $a \approx 0.62$ nm, $c \approx 0.38$ nm, and a value of b which varied with composition. The structures were described in terms of a chemical twinning of a parent structure of the β-U_3O_8 type (*9, 10*). Despite the elegance of this model, a problem exists, as the oxygen-to-metal ratios predicted by the model are greater than those in the real phases. To overcome this difficulty "distortion planes" had to be introduced into the structures. These defects precluded the accurate structure determination usually associated with

0022-4596/91 $3.00

TABLE I

COMPOSITIONS, PREPARATION DETAILS AND c-LINE POSITIONS

Composition	Mol% added oxide	O/M ratio	Conditions (°C/days[a])	c-line $\sin^2\theta$
L-Ta_2O_5				
I	—	2.5000	800/10/P	0.05305
II	—	2.5000	1200/17/P	0.05216
III	—	2.5000	1300[b]/60/P	0.05179
$Ta_2O_5 : Al_2O_3$				
1 : 0.0256	2.50	2.4750	12000/28/P	0.05060
1 : 0.0286	2.78	2.4722	1200/29/P	0.05047
1 : 0.0541	5.13	2.4487	1200/28/P	0.05036
1 : 0.0769	7.14	2.4286	1200/28/P	0.05036[c]
1 : 0.1000	9.09	2.4091	1200/29/P	0.05029[c]
1 : 0.1429	12.50	2.3750	1200/29/P	0.05021[c]
$Ta_2O_5 : TiO_2$				
1 : 0.0571	5.40	2.4861	1200/29/P	0.05194[d]
1 : 0.0571	5.40	2.4861	1120/10/P	0.05121
1 : 0.0833	7.69	2.4800	1200/28/P	0.05179[d]
1 : 0.0833	7.69	2.4800	1120/10/P	0.05108
1 : 0.1429	12.50	2.4667	1200/28/P	0.05165[d]
1 : 0.1429	12.50	2.4667	1120/10/P	0.05104
1 : 0.2000	16.67	2.4545	1200/29/P	—[e]
1 : 0.2222	18.18	2.4500	1200/28/P	—[e]
1 : 0.2857	22.22	2.4375	1200/29/P	—[e]
$Ta_2O_5 : WO_3$				
1 : 0.0541	5.13	2.5132	1350/5/PT	0.05126
1 : 0.0714	6.66	2.5172	1200/17/P	0.05104
1 : 0.0833	7.69	2.5200	1200/17/P	0.05088
1 : 0.1111	10.00	2.5263	1200/17/P	0.05194
1 : 0.1333	11.76	2.5313	1350/5/PT	0.05027
1 : 0.2273	18.52	2.5510	1200/10/ST	0.04932
1 : 0.2727	21.43	2.5600	1200/10/ST	0.04837
1 : 0.3182	24.14	2.5686	1200/10/ST	0.04895
1 : 0.3636[I]	26.66	2.5769	1200/10/ST	0.04886[f]
1 : 0.3636[II]	26.66	2.5769	1350/5/PT	0.04794
$Ta_2O_5 : ZrO_2$				
1 : 0.0351	3.39	2.4914	1200/28/P	0.05225
1 : 0.0541	5.13	2.4868	1200/28/P	0.05241
1 : 0.0721	6.73	2.4826	1200/28/P	0.05276
1 : 0.0870	8.00	2.4792	1200/28/P	0.05359
1 : 0.0989	9.00	2.4764	1200/28/P	0.05341[g]
1 : 0.1111	10.00	2.4737	1200/28/P	0.05325[g]
$Ta_2O_5 : HfO_2$				
1 : 0.0256	2.50	2.4937	1200/28/P	0.05229
1 : 0.0526	5.00	2.4872	1200/28/P	0.05236[h]
1 : 0.0541	5.13	2.4868	1200/28/P	0.05252[h]
1 : 0.0811	7.50	2.4805	1200/28/P	0.05272[h]
1 : 0.0909	8.33	2.4783	1200/28/P	0.05258[h]

TABLE I—*Continued*

COMPOSITIONS, PREPARATION DETAILS AND c-LINE POSITIONS

Composition	Mol% added oxide	*O*/*M* ratio	Conditions (°C/days[a])	*c*-line $\sin^2\theta$
1 : 0.1111	10.00	2.4737	1200/28/P	0.05241[h]
1 : 0.1333	11.76	2.4688	1200/28/P	0.05287[h]
1 : 0.1429	12.50	2.4667	1200/28/P	0.05265[h]
1 : 0.1765	15.00	2.4595	1200/28/P	0.05274[h]
1 : 0.2121	17.50	2.4521	1200/28/P	0.05292[h]
1 : 0.2500	20.00	2.4444	1200/28/P	0.05296[h]
1 : 0.2903	22.50	2.4366	1200/28/P	0.05384[h]
1 : 0.3333	25.00	2.4286	1200/28/P	0.05357[h]
1 : 0.3793	27.50	2.4203	1200/28/P	0.05424[h]
1 : 0.4286	30.00	2.4118	1200/28/P	0.05341[h]
1 : 1.0000	50.00	2.3333	1200/28/P	—[i]

[a] P, Pt boat in air; PT, sealed Pt tube; ST, sealed silica tube.
[b] Sample was air cooled, not liquid nitrogen quenched.
[c] Contained $TaAlO_4$.
[d] Contained H-Ta_2O_5.
[e] H-Ta_2O_5 and $TiTa_2O_7$ only.
[f] Contained Ta_2WO_8.
[g] Contained Ta_6ZrO_{17}.
[h] Contained $Ta_2Zr_6O_{19}$ related phase.
[i] No *L*-Ta_2O_5-type.

X-ray structure analysis and space groups could not be attributed to the phases. To compound the difficulties, many of these *L*-Ta_2O_5 structures yield incommensurate diffraction patterns when examined by electron microscopy (*11–13*), a fact not taken into account in the X-ray studies.

The situation with respect to the crystal chemistry of these compounds therefore remains unsatisfactory. Consequently a number of *L*-Ta_2O_5-related systems, viz., *L*-Ta_2O_5, *L*-Ta_2O_5–Al_2O_3, *L*-Ta_2O_5–TiO_2, *L*-Ta_2O_5–ZrO_2, and *L*-Ta_2O_5–WO_3 and the previously unreported *L*-Ta_2O_5–HfO_2 system, have been reinvestigated by electron diffraction. To compare the present results with previous investigations we have also examined samples using X-ray powder diffraction. It was found that incommensurate diffraction patterns are the norm in all of these systems. The form of the diffraction patterns has been explained in terms of an intergrowth model, although the structures of the units making up the intergrowth have not yet been clarified. The results of our investigations confirm the description of these phases as infinitely adaptive compounds (*2*).

Experimental

Appropriate weights of Johnson Matthey Specpure grade Ta_2O_5 and Al_2O_3, TiO_2, ZrO_2, HfO_2, or WO_3 were mixed by grinding in an agate mortar under Analar grade methanol. They were then dried, pressed into pellets, and either sealed in evacuated silica or platinum tubes or placed on platinum boats. These were subsequently heated at temperatures in the range 800–1350°C for between 5 and 60 days, and then quench cooled in liquid nitrogen, as detailed in Table I.

After firing, all samples were character-

ized by X-ray powder diffraction using a Hägg–Guinier focusing camera and strictly monochromatic Cu$K\alpha_1$ radiation, with KCl (a_0 = 0.6293 nm) as an internal standard. Electron-microscope samples were prepared by crushing small quantities of the samples under *n*-butanol in an agate mortar and then allowing a drop of the resultant suspension to dry on a holey carbon film. Electron diffraction patterns were obtained using a Philips EM400T electron microscope fitted with a side entry double tilt stage and operating at 120 kV.

Results

Powder X-Ray Diffraction

The two main pieces of information obtained from the powder X-ray photographs were the composition range over which the L-Ta_2O_5 structure type persisted, indicated by the presence of other phases, and the position of Moser's *c*-line. These are both summarized in Table I. The phase limits suggested by this work are not precise because no attempt has been made to obtain equilibrium specimens by successive regrinding and heat treatment. In some systems the position of the *c*-line continued to vary smoothly even in the presence of other phases, confirming that equilibrium had not been achieved. This was particularly noticeable in the case of the Ta_2O_5–HfO_2 preparations. The position of the *c*-line is plotted as a function of the parameter L (vide infra) in Fig. 1.

The Ta_2O_5–Al_2O_3 samples showed a consistent *c*-line shift toward lower 2θ-values with increasing Al_2O_3 content, in good agreement with previous work (*1*). This behavior was mirrored in the Ta_2O_5–TiO_2 and Ta_2O_5–WO_3 systems. The opposite behavior was found in the Ta_2O_5–ZrO_2 and Ta_2O_5–HfO_2 systems, where the *c*-line was displaced toward higher 2θ-values as ZrO_2 or HfO_2 was added. Increasing the amount of ZrO_2 beyond 8 mole% resulted in the formation of another phase, which may be Ta_6ZrO_{17} (*1*). No X-ray powder data are available for comparison. Similarly a new phase, possibly related to $Ta_2Zr_6O_{19}$, was observed in the Ta_2O_5–HfO_2 system in samples with compositions richer than 5 mole% in HfO_2.

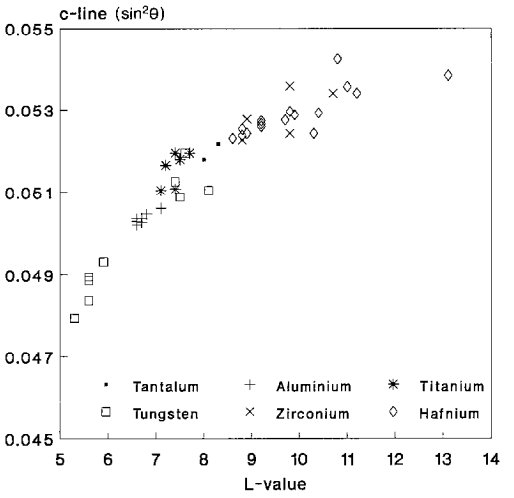

FIG. 1. The relation between *c*-line position and *L*-value; the legend indicates the added metal oxide.

Very little data were obtained concerning the variation of the *c*-line position with temperature in these experiments. The L-Ta_2O_5 samples showed a definite *c*-line shift toward lower 2θ-values with increasing preparation temperature, in agreement with earlier work (*1*, *4*). The same trend was noted in two Ta_2O_5–WO_3 samples, but the Ta_2O_5–TiO_2 samples showed opposite behavior, with the *c*-line position falling as the temperature of sample preparation fell.

Electron Diffraction Patterns

All of the compounds studied gave very similar diffraction patterns, which, in the projection sought, consisted of a peudohexagonal array of strong reflections with rows of closely spaced superlattice reflections grouped around them. The bright spots correspond to the $a'^*b'^*$ projection of the or-

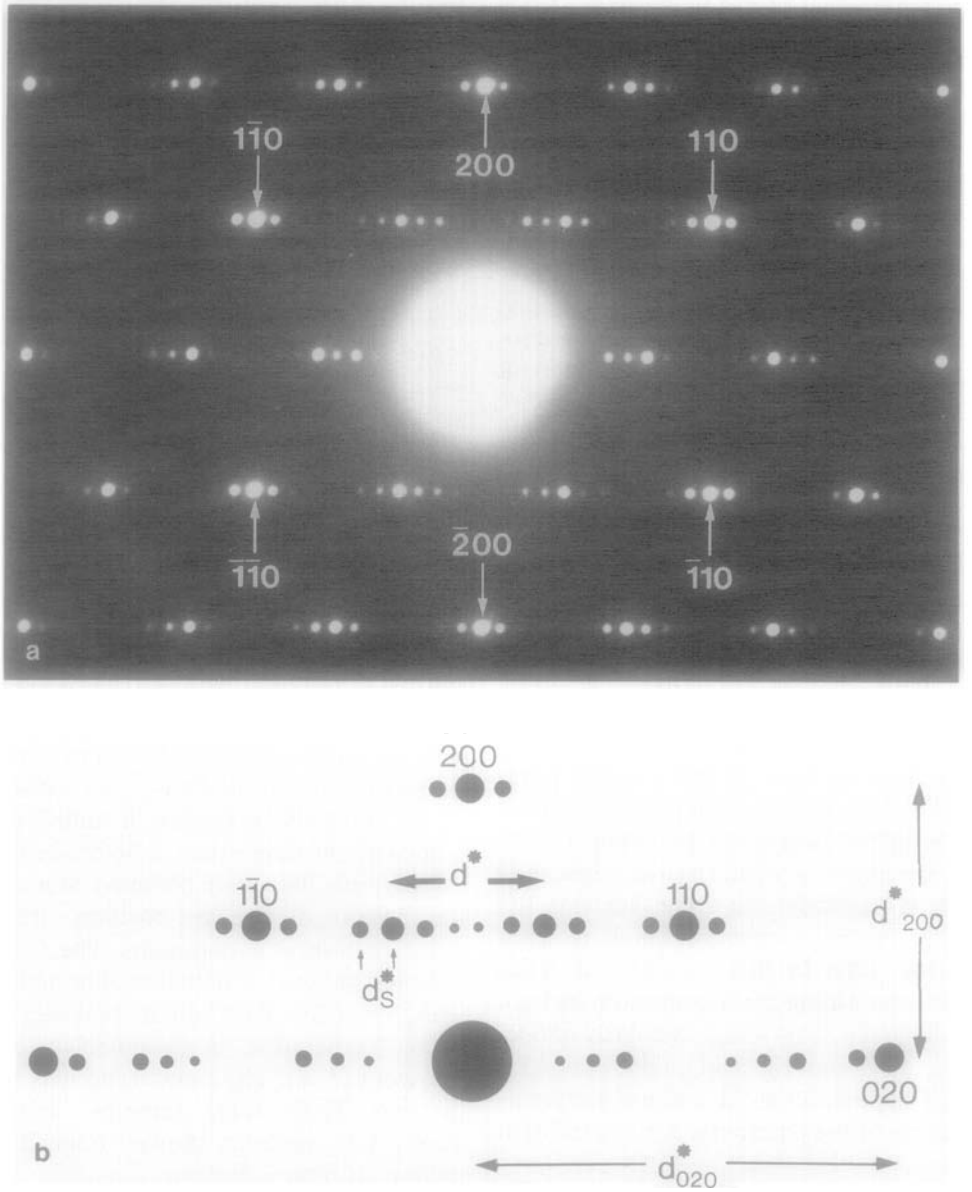

FIG. 2. (a) Electron diffraction pattern of L-Ta_2O_5 indexed in terms of the subcell derived by Lehovec (*3*). (b) A schematic diagram defining the *L*-value in terms of the observed reflections.

thorhombic subcell of *L*-Ta_2O_5 derived by Lehovec (*3*) and can be indexed as shown in Fig. 2a. This section corresponds to the a^*b^* section of the real cell, as a'^* is parallel to a^* and b'^* is parallel to b^*. The rows of superlattice spots lie parallel to the b^*-axis and take the form of clusters of spots associated with each subcell reflection. It is apparent by visual inspection that although each subcell reflection may not be precisely at the center of its associated cluster of spots, it is always the most intense reflection of that

group. The superlattice spots were always sharp and no traces of streaking or diffuse scattering were detected in any of the diffraction patterns of the a^*b^* projection of the unit cell, despite their complexity. None of the patterns observed contained the "orientation anomalies" reported by Spyridelis *et al.* (*11–13*).

Measurement of diffraction patterns revealed that within the clusters of spots there is one unique superlattice-spot spacing for any given pattern. Between the different clusters of spots there is sometimes an integral and more often a nonintegral number of spot spacings; that is, most patterns were incommensurate. Electron diffraction patterns differed from each other in the spacing of the superstructure spots in the b^* direction and the spacing anomaly. For any particular sample, diffraction patterns with a small range of b^*-values were obtained, indicating that the material possessed a range of unit cells.

In order to characterize the extent of the apparent unit cell in the direction parallel to the b-axis, a diagnostic parameter, L, was determined as the ratio d^*/d_s^* as shown in Fig. 2b. This parameter readily allows diffraction patterns to be compared and the trends in diffraction patterns to be followed. The ratio of the b parameter to that of the subcell, b/b', is referred to as the multiplicity, m. An approximate value of m can be obtained from the value of L, as

$$m = 3L - 2. \tag{1}$$

The L-values of a number of diffraction patterns from each sample (usually between 5 and 10) were recorded and the average value taken in order to compensate for the nonequilibrium state of the sample. The L-values obtained are listed in Table II and plotted as a function of the c-line parameter of the sample in Fig. 1.

An accurate value of the b parameter and the multiplicity can also be obtained from the diffraction patterns if the distances d_{200}^* and d_s^* are used. The distances are related to the lattice dimensions by

$$d^* = \lambda l/d, \tag{2}$$

where λl is the camera constant of the electron microscope and d is the relevant interplanar spacing. From Eq. (2),

$$d_s = b = d_{200}d_{200}^*/d_s^*.$$

An accurate value of d_{200} for any sample can be obtained from its X-ray powder pattern.

The results of the electron diffraction analysis are given in Table II. The standard deviation indicates the degree of structural homogeneity in the specimens. The samples show an almost continuous range of average L- and m-values from 5.3 for WO_3-rich Ta_2O_5 : WO_3 samples via 8.0 for L-$Ta_2O_5^{III}$ to $L = 11.2$ for HfO_2-rich Ta_2O_5 : HfO_2 samples. Individual diffraction patterns exhibiting values as high as $L = 16.8$ were found in the $1Ta_2O_5 : 0.2903HfO_2$ sample.

Although the diffraction patterns were complex and the data reported in Table II suggest that a continuous range of L and multiplicity values, m, existed, visual examination of the diffraction patterns showed that they fell into a smaller number of underlying base types, characterized by multiplicity values of 13, 16, 19, 22, 25, 28, 31, and 34. The most oxygen rich materials, typified by the L-Ta_2O_5–WO_3 system, give rise to diffraction patterns corresponding to a preponderence of m-values of 13, 16, and 19 while the most oxygen poor materials typified by the L-Ta_2O_5–HfO_2 and L-Ta_2O_5–ZrO_2 systems correspond to m-values of 25 and greater. L-Ta_2O_5 itself seems not to be unique, but falls in the middle of the sequence range.

Interpretation

A reasonable model for the continuum of phases that gives rise to the incommensu-

rate diffraction patterns and the apparent continuous range of L- and m-values assumes that the complex unit cells consist of ordered intergrowths of varying proportions of two neighboring base units, for example, 13 + 16, 16 + 19, and so on.

A simplified analysis of this situation is possible using methods derived previously (*14*). This is achieved by representing an intergrowth by an appropriately positioned set of delta functions and analyzing the expected Fraunhofer diffraction pattern from the array using conventional Fourier transform methods (*15*), as follows. For a one-dimensional array of N unit-height delta functions, with x-coordinates $a_1, a_2, \ldots, a_N$, represented by

$$f(x) = \sum_p \delta(x - a_p)$$

the Fourier transform relation

$$F(u) = \int_{-\infty}^{+\infty} f(x)e^{-2\pi iux}dx$$

simplifies to a series of N terms given by

$$F(u) = \sum_{p=1}^{N} e^{(-2\pi iua_p)},$$

where $F(u)$ is the amplitude of the diffraction pattern at position u. The intensity of the pattern is given by

$$I(u) = F^*(u) \cdot F(u),$$

where $F^*(u)$ is the complex conjugate of the amplitude. Therefore

$$\begin{aligned} I(u) &= \sum_{p=1}^{N} e^{(2\pi iua_p)} \cdot \sum_{q=1}^{N} e^{(-2\pi iua_q)} \\ &= \sum_{p=1}^{N} \sum_{q=1}^{N} e^{2\pi iu(a_p - a_q)} \\ &= N + \sum_{p=1}^{N-1} \sum_{q=p+1}^{N} 2\cos 2\pi u(a_p - a_q), \end{aligned}$$

where the summation consists of $N(N - 1)/2$ terms.

The expected intensities of the electron diffraction patterns were calculated from this comparatively simple equation by choosing arrays of delta functions corresponding to the m values determined experimentally. Initially diffraction patterns were calculated for evenly spaced arrays of delta functions separated by repeat distances of 13, 16, 19, 22, 25, 28, 31, and 34. These were found to be in good agreement with the experimental diffraction patterns found for the commensurate underlying base types.

To calculate incommensurate diffraction patterns arrays of delta functions containing more than one of these base spacings were employed. The notation used to characterize the sequences is typified by 19^922^1, which means an array of 9 separations of 19 followed by 1 separation of 22. Calculations revealed that the arrangement of the component units of the sequences had a great influence upon the form of the diffraction pattern intensities. For example, the diffraction pattern from a sequence 19^322^7, that is 3 spacings of 19 one after the other followed by 7 spacings of 22 is very different from that generated by the sequence $22^219^122^219^122^219^122$, where the spacings of 19 are distributed fairly evenly, although each pattern has the same overall repeat parameters, $L = 7.7$, $m = 21.1$. Because of this specificity all of the experimentally obtained diffraction patterns could be linked to unique stacking sequences.

To illustrate this point several incommensurate electron diffraction patterns along with their computer simulations are shown in Fig. 3. The strong reflections on the electron diffraction patterns correspond to the (110) and $(1\bar{1}0)$ spots, as shown in Fig. 2a. The intensities of the corresponding calculated reflections are represented by vertical lines of the appropriate height and are correctly scaled and positioned with respect to the experimental patterns. It is seen that there is good agreement between the two

TABLE II

ELECTRON MICROSCOPE PHASE ANALYSIS

Composition	L	m	No	$\bar{L} \pm \sigma(L)$	$\bar{m} \pm \sigma(m)$	Typical stacking sequence
$L - Ta_2O_5$						
II	8.2	22.6	1	8.3 ± 0.1	23.0 ± 0.3	22 + 25
	8.3	22.9	3			
	8.5	23.5	1			
III	7.9	21.7	2	8.0 ± 0.1	22.1 ± 0.4	22
	8.0	22.0	1			
	8.2	22.6	2			
$Ta_2O_5 : Al_2O_3$						
1 : 0.0256	7.1	19.3	8	7.1 ± 0.1	19.3 ± 0.1	19 + 22
	7.2	19.6	1			
1 : 0.0286	6.7	18.1	1	6.8 ± 0.1	18.4 ± 0.1	16 + 19
	6.8	18.4	6			
1 : 0.0541	6.4	17.2	1	6.7 ± 0.1	17.9 ± 0.3	16 + 19
	6.6	17.8	1			
	6.7	18.1	3			
1 : 0.0769	6.6	17.8	4	6.6 ± 0.1	17.9 ± 0.1	16 + 19
	6.7	18.1	1			
1 : 0.1	6.6	17.8	6	6.6 ± 0.1	17.8 ± 0.1	16 + 19
	6.7	18.1	1			
1 : 0.1429	6.5	17.5	3	6.6 ± 0.1	17.7 ± 0.3	16 + 19
	6.6	17.8	1			
	6.8	18.4	1			
$Ta_2O_5 : TiO_2$ (1200°C)						
1 : 0.0571	7.6	20.8	1	7.7 ± 0.1	21.1 ± 0.1	19 + 22
	7.7	21.1	5			
1 : 0.0833	7.5	20.5	7	7.5 ± 0.1	20.5 ± 0.1	19 + 22
	7.6	20.8	1			
1 : 0.1429	7.1	19.3	5	7.2 ± 0.1	19.5 ± 0.3	19 + 22
	7.2	19.6	1			
	7.3	19.9	1			
	7.4	20.2	1			
(1120°C)						
1 : 0.0571	7.3	19.9	1	7.4 ± 0.1	20.3 ± 0.2	19 + 22
	7.4	20.2	4			
	7.5	20.5	3			
1 : 0.0833	7.2	19.6	2	7.4 ± 0.1	20.1 ± 0.4	19 + 22
	7.3	19.9	2			
	7.4	20.2	1			
	7.5	20.5	4			
1 : 0.1429	7.0	19.0	2	7.1 ± 0.1	19.3 ± 0.2	19 + 22
	7.1	19.3	2			
	7.2	19.6	2			
$Ta_2O_5 : WO_3$						
1 : 0.0541	7.4	20.2	3	7.4	20.2	19 + 22
1 : 0.0714	8.0	22.0	3	8.1 ± 0.1	22.4 ± 0.4	22 + 25
	8.2	22.6	1			
	8.3	22.9	2			

TABLE II—*Continued*

ELECTRON MICROSCOPE PHASE ANALYSIS

Composition	L	m	No	$\bar{L} \pm \sigma(L)$	$\bar{m} \pm \sigma(m)$	Typical stacking sequence
1 : 0.0833	7.3	19.9	1	7.5 ± 0.1	20.5 ± 0.4	19 + 22
	7.4	20.2	2			
	7.5	20.5	2			
	7.6	20.8	1			
	7.7	21.1	2			
1 : 0.1111	7.0	19.0	1	7.6 ± 0.4	20.7 ± 1.1	19 + 22
	7.3	19.9	1			
	7.4	20.2	1			
	7.7	21.1	2			
	8.2	22.6	1			
1 : 0.1333	6.7	18.1	3	6.7	18.1	16 + 19
1 : 0.2273	5.8	15.4	2	5.9 ± 0.1	15.8 ± 0.3	13 + 16
	6.0	16.0	4			
1 : 0.2727	5.5	14.5	2	5.6 ± 0.1	14.7 ± 0.2	13 + 16
	5.6	14.8	2			
1 : 0.3182	5.5	14.5	1	5.6 ± 0.1	14.7 ± 0.1	13 + 16
	5.6	14.8	4			
1 : 0.3636[I]	5.6	14.8	3	5.6	14.8	13 + 16
1 : 0.3636[II]	5.3	13.9	3	5.3	13.9	13 + 16
$Ta_2O_5 : ZrO_2$						
1 : 0.0351	8.7	24.1	3	8.8 ± 0.1	24.3 ± 0.2	22 + 25
	8.8	24.4	3			
1 : 0.0541	7.9	21.7	1	9.8 ± 1.1	27.5 ± 3.4	25 ± 28
	9.1	25.3	1			
	9.3	25.9	1			
	9.6	26.8	1			
	9.8	27.4	1			
	10.2	28.6	1			
	10.8	30.4	1			
	12.0	34.0	1			
1 : 0.0721	8.5	23.5	1	8.9 ± 0.4	24.7 ± 1.1	22 + 25
	8.7	24.1	1			
	8.8	24.4	3			
	8.9	24.7	1			
	9.7	27.1	1			
1 : 0.0870	9.8	27.4	2	9.8 ± 0.1	27.5 ± 0.1	25 + 28
	9.9	27.7	1			
1 : 0.0989	9.9	27.7	1	10.7 ± 0.8	30.0 ± 2.3	28 + 31
	11.4	32.2	1			
1 : 0.1111	9.7	27.1	1	10.3 ± 0.6	29.0 ± 1.9	28 + 31
	10.1	28.3	1			
	11.2	31.6	1			
$Ta_2O_5 : HfO_2$						
1 : 0.0256	8.5	23.5	1	8.6 ± 0.1	23.9 ± 0.3	22 + 25
	8.6	23.8	4			
	8.7	24.1	1			
	8.8	24.4	1			
1 : 0.0526	8.6	23.8	1	8.8 ± 0.1	24.4 ± 0.4	22 + 25
	8.7	24.1	2			
	8.8	24.4	1			
	8.9	24.7	2			
	9.0	25.0	1			

TABLE II—*Continued*

ELECTRON MICROSCOPE PHASE ANALYSIS

Composition	L	m	No	$\bar{L} \pm \sigma(L)$	$\bar{m} \pm \sigma(m)$	Typical stacking sequence
1:0.0541	8.7	24.1	4	8.8 ± 0.1	24.4 ± 0.5	22 + 25
	8.9	24.7	1			
	9.1	25.3	1			
1:0.0811	8.8	24.4	3	9.2 ± 0.7	27.5 ± 6.0	25 + 28
	8.9	24.7	1			
	10.5	39.5	1			
1:0.0909	8.7	24.1	1	9.2 ± 0.3	25.5 ± 0.9	25 + 28
	8.9	24.7	2			
	9.3	25.9	1			
	9.4	26.2	1			
	9.5	26.5	2			
1:0.1111	8.5	23.5	1	8.9 ± 0.4	24.7 ± 1.2	22 + 25
	8.6	23.8	1			
	8.7	24.1	2			
	8.8	24.4	1			
	9.2	25.6	1			
	9.7	27.1	1			
1:0.1333	9.0	25.0	1	9.9 ± 1.0	27.6 ± 2.9	25 + 28
	9.1	25.3	1			
	9.7	27.1	1			
	9.9	27.7	1			
	11.7	33.1	1			
1:0.1429	9.1	25.3	1	9.2 ± 0.1	25.8 ± 0.5	25 + 28
	9.2	25.6	2			
	9.5	26.5	1			
1:0.1765	8.1	22.3	1	9.7 ± 1.1	27.0 ± 3.2	25 + 28
	9.3	25.9	1			
	10.4	29.2	1			
	10.8	30.4	1			
1:0.2121	9.1	25.3	1	10.4 ± 0.7	29.1 ± 2.2	28 + 31
	9.6	26.8	1			
	10.3	28.9	1			
	10.5	29.5	2			
	11.2	31.6	1			
	11.3	31.9	1			
1:0.25	8.2	22.6	1	9.8 ± 0.9	27.5 ± 2.6	25 + 28
	9.2	25.6	1			
	9.7	27.1	2			
	9.9	27.7	1			
	10.0	28.0	1			
	10.5	29.5	1			
	11.4	32.2	1			
1:0.2903	10.0	28.0	1	13.1 ± 2.8	37.4 ± 8.4	37 + 40
	12.6	35.8	1			
	16.8	48.4	1			
1:0.3333	10.3	28.9	1	11.0 ± 0.6	30.9 ± 1.9	31
	10.8	30.4	1			
	11.8	33.4	1			
1:0.3793	10.8	30.4	1	10.8	30.4	28 + 31
1:0.4286	10.2	28.6	1	11.2 ± 0.7	31.5 ± 2.1	31 + 34
	11.6	32.8	1			
	11.7	33.1	1			

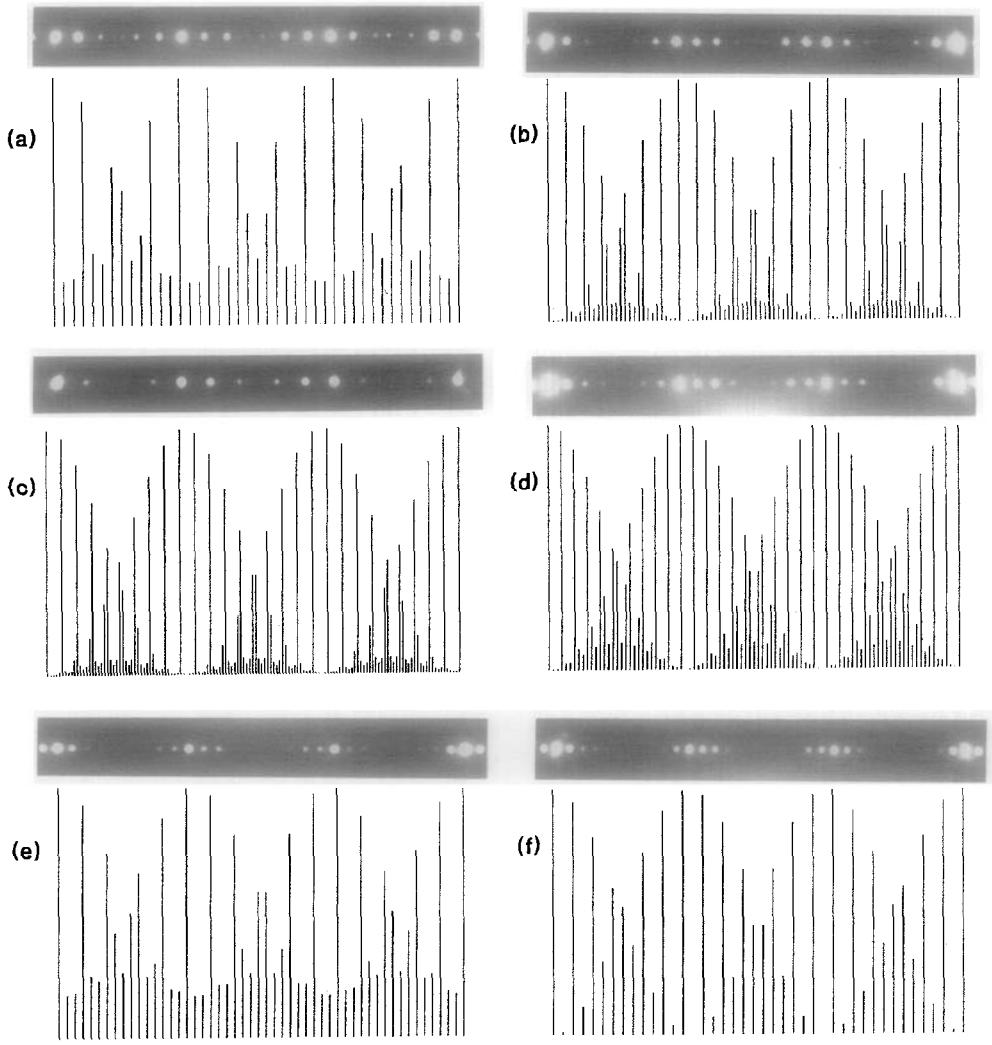

FIG. 3. Incommensurate electron diffraction patterns (above) and corresponding computed simulations (below); (a) from sample $1Ta_2O_5 : 0.3636WO_3$ II, sequence 13^216^1; (b) from sample L-Ta_2O_5 II, sequence 22^325^1; (c), from sample $1Ta_2O_5 : 0.0989ZrO_2$, sequence 28^425^1; (d), from sample $1Ta_2O_5 : 0.2121HfO_2$, sequence 31^234^1; (e), from sample $1Ta_2O_5 : 0.1000Al_2O_3$, sequence 16^219^1; (f), from sample $1Ta_2O_5 : 0.0833TiO_2$ 1120°C, sequence 16^119^1.

sets of data, from the point of view of both the relative intensities and the generation of spacing anomalies in the correct positions.

Discussion

The X-ray diffraction results are in complete agreement with earlier work (*1*, *4*), both in terms of the extent of the phase range of the *L*-Ta_2O_5 structure type and the shift of the diagnostic *c*-line. The data show that the *c*-line shifts smoothly and continuously with the amount of added metal oxide up to the phase boundary of that system. The direction of movement of the *c*-line and the magnitude of the shift differs according to

the particular oxide added to the L-Ta_2O_5, moving toward lower values of 2θ for Al_2O_3, TiO_2, and WO_3 and toward higher values of 2θ in the cases of ZrO_2 and HfO_2.

Moser (*4*) believed that the c-line was indicative of the structure of the sample but Stephenson and Roth (*5–8*) were unable to relate it to the superstructure of the unit cells that they derived in the Ta_2O_5–WO_3 system. The electron diffraction patterns obtained in this study showed conclusively that all samples were inhomogeneous on a microstructural scale. This precludes indexing the c-line reflection uniquely and thus attaching any precise crystallographic significance to its position. However, the smooth variation in the position of this line with composition, as indicated by Fig. 1, allows it to be used to assess the overall composition of the L-Ta_2O_5 phase in a reasonably quantitative fashion. However, as the results show that the microstructures observed varied with preparation temperature, the relationship must be used cautiously.

The electron diffraction patterns reveal that the structures forming in the systems studied are complex. However, despite the large number of different and very long unit cell phases identified, no traces of diffuse scattering or streaking were recorded on the a^*b^* reciprocal lattice sections obtained, and hence the phases conform well to Anderson's original description of them as infinitely adaptive structures (*2*). It is clear that the parameter L and the multiplicity m are influenced by a number of factors including composition and temperature. It is also clear that L-Ta_2O_5 is not unique, but exists as a group of structures within the phase range of the structure type.

Although the samples examined in the present study are not necessarily at equilibrium, the nominal oxygen-to-metal ratio of each sample, shown in Table I, reveals that the structure type extends from approximately $MO_{2.5769}$ for $11Ta_2O_5:4WO_3$ to

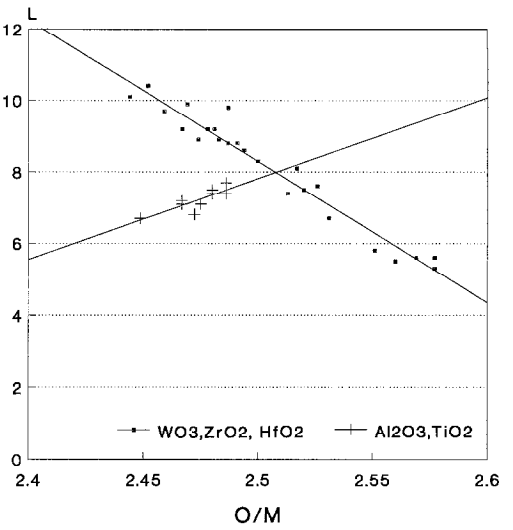

FIG. 4. The relationship between the L-value and O/M, the oxygen-to-metal ratio, in the L-Ta_2O_5-type phases; the legend indicates the added metal oxide.

$MO_{2.4118}$ for $7Ta_2O_5:3HfO_2$, corresponding to m-values of 13 to 34, respectively. These composition limits are temperature dependent. As shown in Fig. 4, L decreases continuously with increasing oxygen content in the Ta_2O_5–HfO_2, Ta_2O_5–ZrO_2, and Ta_2O_5–WO_3 systems. Data for L-Ta_2O_5, $MO_{2.5000}$, shows it to lie on the same line. It would therefore seem that a correlation exists between structure and stoichiometry with an increasing oxygen content corresponding to a decreasing b-lattice parameter. However, two systems appear anomalous, with the Ta_2O_5–TiO_2 and Ta_2O_5–Al_2O_3 systems exhibiting a reverse trend.

Further studies, particularly at an atomic level of discrimination, are needed to resolve this problem. Additionally, the fact that in this study all diffraction patterns show only rows of superlattice spots parallel to the b-axis, and no tilted rows displaying "orientation anomalies" needs to be explored further. These aspects will be considered in a future publication.

Acknowledgment

One of the authors (J.M.W.) acknowledges with gratitude the tenure of a University of Wales research studentship.

References

1. R. S. Roth and J. L. Waring, *J. Res. Natl. Bur. Stand. Sect. A* **74,** 485 (1970).
2. J. S. Anderson, *J. Chem. Soc. Dalton Trans.* 1107 (1973).
3. K. Lehovec, *J. Less-Common Met.* **7,** 397 (1964).
4. R. Moser, *Schweiz. Mineral. Petrogr. Mitt.* **45,** 35 (1965).
5. N. C. Stephenson and R. S. Roth, *Acta. Crystallogr. Sect. B* **27,** 1010 (1971).
6. N. C. Stephenson and R. S. Roth, *Acta. Crystallogr. Sect. B* **27,** 1018 (1971).
7. N. C. Stephenson and R. S. Roth, *Acta. Crystallogr. Sect. B* **27,** 1037 (1971).
8. N. C. Stephenson and R. S. Roth, *Acta. Crystallogr. Sect. B* **27,** 1037 (1971).
9. F. Andresen, *Acta. Crystallogr.* **11,** 612 (1958).
10. R. S. Roth and N. C. Stephenson, "The Chemistry of Extended Defects in Non-Metallic Solids," (L. Eyring and M. O'Keefe Eds.), p. 167, North-Holland, Amsterdam (1970).
11. J. Spyridelis, P. Delavignette, and S. Amelinckx, *Mater. Res. Bull.* **2,** 113 (1967).
12. J. Spyridelis, P. Delavignette, and S. Amelinckx, *Phys. Stat. Sol.* **19,** 683 (1967).
13. J. Spyridelis, P. Delavignette, and S. Amelinckx, *Mater. Res. Bull.* **3,** 31 (1968).
14. D. Mercurio, B. Frit, G. Harburn, B. H. Parry, R. P. Williams, and R. J. D. Tilley, *Phys. Stat Sol A* **108,** 111 (1988).
15. R. N. Bracewell, "Fourier Transform and Its Applications," McGraw-Hill Publishing Co. (1978).